

Unified Structural–Hydrodynamic Modeling of Underwater Underactuated Mechanisms and Soft Robots

Chenrui Zhang^{1†}, Graduate Student Member, IEEE, Yiyuan Zhang^{1,2†*}, Graduate Student Member, IEEE, Yunfei Ye¹, Junkai Chen¹, Haozhe Wang^{1,2} and Cecilia Laschi¹, Fellow, IEEE

Abstract—Underwater robots are widely deployed for ocean exploration and manipulation. Underactuated mechanisms are particularly advantageous in aquatic environments, as reducing actuator count lowers the risk of motor leakage while introducing inherent mechanical compliance. However, accurate modeling of underwater underactuated and soft robotic systems remains challenging because it requires identifying a high-dimensional set of internal structural and external hydrodynamic parameters. In this work, we propose a trajectory-driven global optimization framework for unified structural–hydrodynamic modeling of underwater multibody systems. Inspired by the Covariance Matrix Adaptation Evolution Strategy (CMA-ES), the proposed approach simultaneously identifies coupled internal elastic, damping, and distributed hydrodynamic parameters through trajectory-level matching between simulation and experimental motion. This enables high-fidelity reproduction of both underactuated mechanisms and compliant soft robotic systems in underwater environments. We first validate the framework on a link-by-link underactuated multibody mechanism, demonstrating accurate identification of distributed hydrodynamic coefficients, with a normalized end-effector position error below 5% across multiple trajectories, varying initial conditions, and both active–passive and fully passive configurations. The identified modeling strategy is then transferred to a single octopus-inspired soft arm, showing strong real-to-sim consistency without manual retuning. Finally, eight identified arms are assembled into a swimming octopus robot, where the unified parameter set enables realistic whole-body behavior without additional parameter calibration. These results demonstrate the scalability and transferability of the proposed structural–hydrodynamic modeling framework across underwater underactuated and soft robotic systems.

I. INTRODUCTION

Our world is mostly covered by water, which is abundant in resources and contains many fascinating unknowns [1]. Over the past decades, underwater robots have been increasingly adopted for underwater exploration to ensure the safety of human divers while enhancing human capability [2], [3]. Substantial knowledge has been accumulated in the

design of underwater manipulators and vehicles, extending human capability in underwater manipulation, underwater locomotion, and observation [4]. Underactuated mechanisms are particularly advantageous for underwater robotic systems, as they reduce the number of required actuators, thereby lowering the risk of motor leakage and improving structural compliance and robustness in complex aquatic environments [5]. Most aquatic animals, such as fish, sea lions, penguins, octopuses, and even worms, possess soft-bodied structures. At the same time, reducing actuator numbers and developing underactuated approaches. Bio-inspired soft robots derived from these organisms have therefore become a promising approach for developing improved underwater manipulators and swimming robots (vehicles) [6], [7]. However, efficient modeling of the soft body itself is already a state-of-the-art research topic. Incorporating the hydrodynamics model of the surrounding fluid further increases the difficulty [8], [9], [10], [11], [12], where the hydrodynamics parameters typically relies on conventional computational fluid dynamics (CFD) methods [13], experimental method [14] and further model-based identification [8], [11], [12].

Inspired by the well-known efficient simplification pseudo-rigid approach [15] (the soft bodies are represented as series of rigid links, which are connected by joints) in soft robot modeling, researchers have begun developing robots in a similar discrete-body manner to facilitate direct modeling within the pseudo-rigid framework [16], [17]. By leveraging the speed and accuracy advantages of the MuJoCo multibody simulator [18] and using preset mechanical parameters, these models show strong similarity between simulation and real robot manipulation. This provides an opportunity to share existing tools and knowledge between soft robots and underactuated multibody systems.

In air, the current multibody simulation approaches can still be adjusted satisfactorily through manual tuning [19] or differential evolution–based staged optimization [17] for bending stiffness and damping coefficient as internal soft body metrics. In water, however, the problem becomes significantly more challenging due to the introduction of hydrodynamics parameters, including blunt drag coefficient, slender drag coefficient, angular drag coefficient, kutta lift coefficient, and magnus lift coefficient. With such a high order of internal soft body dynamics parameters combined with external fluid environment dynamics parameters, especially in the underactuated and pseudo-rigid systems, manual or staged optimization approaches are no longer sufficient to characterize the physical dynamics parameters of underwater

[†]These authors contributed equally to this work.

*Corresponding author: Yiyuan Zhang (yiyuan.zhang@u.nus.edu)

¹Department of Mechanical Engineering and Advanced Robotics Centre, National University of Singapore, Singapore.

²Singapore-MIT Alliance for Research and Technology (SMART) Centre, 138602, Singapore.

This work was supported by following projects: the DESTRO project (“Dextrous, strong yet soft robots,” R22I0IR124), funded by MAE (Italy) and A*STAR (Singapore); the REBOT project (“Rethinking underwater robot manipulation,” Moe-t2eP50221-0010), funded by the Singapore Ministry of Education; and also the National Research Foundation, Prime Ministers Office, Singapore under its Campus for Research Excellence and Technological Enterprise (CREATE) programme. The Mens, Manus, and Machina (M3S) is an interdisciplinary research group of the Singapore MIT Alliance for Research and Technology (SMART) centre.

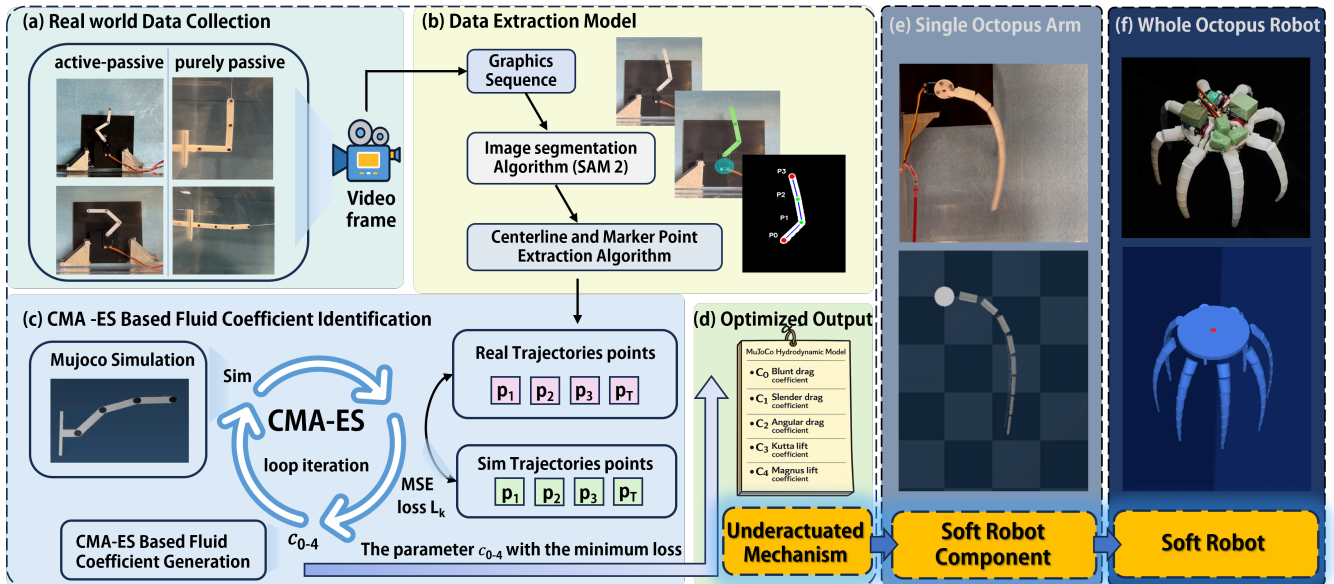


Fig. 1. Trajectory-driven CMA-ES framework for simultaneous identification of distributed hydrodynamic coefficients, validated from a three-link mechanism to an octopus-inspired arm and an eight-arm robot. **(a) Real-world data collection:** Underwater trajectories are recorded using an active-passive coupled three-link mechanism and a purely passive mechanism. **(b) Data extraction:** SAM2-based segmentation and centerline extraction are used to obtain key trajectory points from experimental videos. **(c) Fluid coefficient identification:** Real trajectories are matched with MuJoCo simulations, and CMA-ES iteratively optimizes hydrodynamic parameters to minimize trajectory error. **(d) Optimized output:** The identified hydrodynamic coefficient set c_0 - c_4 calibrates the underwater dynamics model. **(e) Soft robot component:** The identified parameters are applied to a single octopus-inspired arm to evaluate parameter transferability. **(f) Soft robot:** Multiple identified arms are arranged in a circular configuration to construct an octopus-inspired robot, demonstrating scalability.

soft and underactuated robots.

Inspired by the CMA-ES method applied to humanoid robots [20], a powerful multibody dynamics parameter optimization approach, can globally optimize mass-inertia parameters and actuator model parameters in the optimal stage. Considering the overlapping and sharing of well-deployed underwater underactuated multibody systems within embodied intelligent modeling for soft robots starting from the pseudo-rigid approach, we begin with four cases of a passive three-link mechanism, which is the conventional starting point in underwater manipulator modeling. We establish a unified trajectory-driven global optimization framework to simultaneously identify distributed hydrodynamic coefficients of underwater underactuated multibody systems. The framework achieves high-fidelity reproduction of real-world motion trajectories, including direction-dependent asymmetric dynamics, demonstrating strong sim-to-real consistency across mechanism, component, and full-robot levels.

Based on the embodied dynamics connection between underactuated mechanisms and soft robotics, especially robots designed in a discrete-body manner, we apply the same approach to an octopus swimming-inspired arm [21]. The results show strong resemblance and accuracy of reproduction of real-world motion trajectories and consistent direction-dependent dynamic responses. After verifying our underactuated multibody internal and external hydrodynamics parameter identification approach on the soft arm, we directly arrange eight identical identified arms in a circular configuration to assemble an octopus swimming-like robot.

The assembled system shows strong visual resemblance to the real robot without further parameter fine-tuning.

Through this work, we aim to highlight our contribution to underwater robotics by empowering underwater underactuated system parameter identification with the latest global optimization approach, which enables simultaneous estimation of coupled parameters at the trajectory level. Furthermore, this work establishes hydrodynamics-based connection between underwater underactuated mechanisms and underwater soft robot pseudo-rigid modeling. By unifying internal structural dynamics and external fluid dynamic parameters within a single identification framework, we provide a systematic solution that bridges two traditionally separated modeling communities. Considering the advantages of underwater underactuated robots and soft robots as mentioned above, together with the demonstrated octopus eight-arm swimming resemblance, we envision that our framework will serve as an impactful and reusable approach for both the underwater underactuated robotics community and the underwater soft robotics community.

II. METHODS

A. Underactuated Mechanism Experimental Platforms

This study focuses on the dynamic behaviors of underactuated underwater mechanisms. To systematically investigate active-passive underactuated coupling and purely passive hydrodynamic responses, two experimental platforms with distinct actuation configurations were developed.

The first platform, shown in Fig. 2(a), implements an active-passive coupled transmission structure. A motor directly actuates the first link segment, constituting the active component, while the subsequent links are not independently actuated and are mechanically connected to the driven segment. These downstream links interact with the surrounding fluid purely through passive dynamics induced by the upstream actuation. This configuration exhibits a high kinematic degree of freedom with a limited number of actuators, representing a canonical underactuated robotic structure. Therefore, it serves as a representative testbed for studying fluid-structure interactions in actively driven underactuated underwater robots.

To ensure safe and stable underwater operation, the motor and electronic components were waterproofed. Electrical connections were insulated and sealed using heat-shrink tubing to prevent water intrusion.

The second platform, shown in Fig. 2(b), represents a purely passive configuration. A supporting line initially holds the distal end of the uppermost link such that it maintains a perpendicular orientation relative to the second link. At the start of each experiment, the support line is released, allowing the multi-link structure to move freely under gravity without any active control input. The base frame is rigidly fixed to the sidewall of the water tank. This configuration enables evaluation of the intrinsic passive hydrodynamic response and provides baseline data for subsequent model validation and parameter identification.

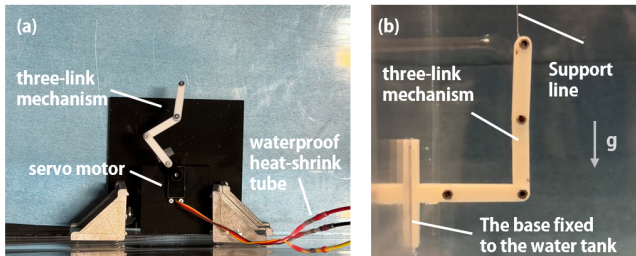


Fig. 2. Three-link mechanism setup

B. Real-world Trajectory Extraction

To obtain ground-truth motion trajectories (Fig. 3), we developed a vision-based trajectory extraction pipeline combining video segmentation and skeleton-based keypoint detection.

After each experiment, underwater motion was recorded using a fixed camera. The recorded video was converted into a sequence of image frames, where Fig. 3(a) illustrates a representative frame. The moving three-link structure was segmented using the SAM2 model [22], and the detailed procedure is described in Algorithm 1. As shown in Fig. 3(b), the dynamically captured link mask is highlighted in green, while the initial mask is indicated in blue.

Following segmentation, a skeletonization algorithm was applied to the binary mask to extract the medial axis of the link structure. Key trajectory points were then defined along

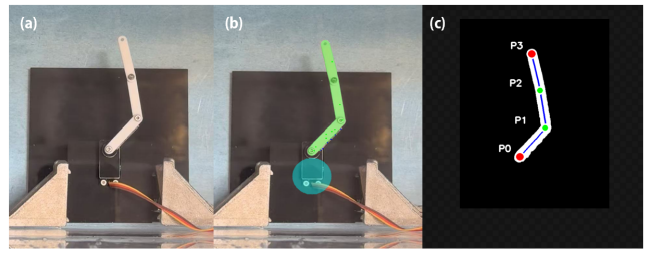


Fig. 3. Vision-based trajectory extraction for the three-link mechanism

the extracted centerline. For the motor-driven configuration, the lowest endpoint was defined as the reference P_0 ; for the gravity-driven passive configuration, the leftmost endpoint was defined as P_0 . The distal endpoint of the structure was defined as P_3 . The centerline was subsequently divided into three equal segments to determine intermediate keypoints P_1 and P_2 . In visualization, the two endpoints are marked in red, while the intermediate points are marked in green.

This processing pipeline was executed for all frames in the image sequence, resulting in time-series trajectory data that serve as ground truth for subsequent physical parameter identification and model validation.

Algorithm 1 Trajectory Extraction via SAM2-based Video Segmentation

Require: Image sequence $\{I_t\}_{t=0}^T$, static region mask S , user clicks P

Ensure: Object trajectory $\mathcal{T} = \{p_t\}_{t=0}^T$

- 1: Initialize SAM2 video predictor \mathcal{P}
 - 2: Select start frame k and collect user annotations P
 - 3: Initialize predictor with (I_k, P) and obtain initial object mask M_k
 - 4: Extract initial trajectory point $p_k \leftarrow \text{CENTROID}(M_k \wedge \neg S)$
 - 5: **for** $t = k + 1$ **to** T **do**
 - 6: Propagate object mask $M_t \leftarrow \mathcal{P}(I_t | M_{t-1})$
 - 7: Remove static regions: $\tilde{M}_t \leftarrow M_t \wedge \neg S$
 - 8: Extract trajectory point $p_t \leftarrow \text{CENTROID}(\tilde{M}_t)$
 - 9: **end for**
 - 10: $\mathcal{T} \leftarrow \{p_k, p_{k+1}, \dots, p_T\}$
 - 11: **return** \mathcal{T}
-

C. CMA-ES Based Fluid Coefficient Identification

The physical parameter identification problem is formulated as a trajectory-matching optimization task. The objective is to recover hydrodynamic coefficients by minimizing the discrepancy between real-world and simulated trajectories.

1) *Parameter Modeling:* Consider an articulated underwater system composed of n rigid links. Each link is associated with one observation point and characterized by five hydrodynamic coefficients. The complete parameter vector is defined as

$$\mathbf{x} = [\mathbf{c}_1^\top \quad \mathbf{c}_2^\top \quad \cdots \quad \mathbf{c}_n^\top]^\top \in \mathbb{R}^{5n}, \quad (1)$$

where $\mathbf{c}_i \in \mathbb{R}^5$ denotes the fluid coefficient vector of the i -th link.

Given a parameter vector \mathbf{x} , the MuJoCo forward dynamics simulation produces a trajectory

$$T_{\text{sim}}(\mathbf{x}) = \{\mathbf{y}(t)\}_{t=1}^N \in \mathbb{R}^{N \times 3n}, \quad (2)$$

where $\mathbf{y}(t)$ stacks the positions of all observation points at time step t . The corresponding real-world trajectory is denoted as T_{real} .

2) *Loss Function and Optimization Objective:* The discrepancy between simulated and real trajectories is quantified using the mean squared error (MSE):

$$L(\mathbf{x}) = \frac{1}{N} \sum_{t=1}^N \|\mathbf{y}_{\text{sim}}(t; \mathbf{x}) - \mathbf{y}_{\text{real}}(t)\|^2. \quad (3)$$

The parameter identification problem is therefore formulated as

$$\mathbf{x}^* = \arg \min_{\mathbf{x}} L(\mathbf{x}), \quad \text{s.t.} \quad \mathbf{b}_{\min} \leq \mathbf{x} \leq \mathbf{b}_{\max}, \quad (4)$$

where \mathbf{b}_{\min} and \mathbf{b}_{\max} define physically feasible bounds.

3) *CMA-ES-Based Optimization:* Due to the highly non-linear and non-differentiable nature of fluid–structure interactions in underwater dynamics, gradient-based methods are not suitable. Therefore, we employ the Covariance Matrix Adaptation Evolution Strategy (CMA-ES) for derivative-free global optimization.

At generation g , candidate solutions are sampled from a multivariate normal distribution:

$$\mathbf{x}_k^{(g)} \sim \mathcal{N}\left(\mathbf{m}^{(g)}, \left(\sigma^{(g)}\right)^2 \mathbf{C}^{(g)}\right), \quad k = 1, \dots, \lambda. \quad (5)$$

For each sampled parameter vector, the following steps are performed:

- The parameters are loaded into the MuJoCo model;
- Forward dynamics simulation is executed;
- The trajectory loss $L(\mathbf{x})$ is computed;
- The sampling distribution is updated according to fitness ranking.

D. Optimized Output

The optimization is performed for up to 5000 iterations, yielding the parameter set \mathbf{x}^* that minimizes the trajectory discrepancy. The overall real-to-sim identification framework is illustrated in Fig. 1(c), and implementation details are provided in Algorithm 2.

This approach establishes a closed-loop trajectory-driven simulation calibration framework, forming the foundation of the proposed real-to-sim system.

After iterative optimization, CMA-ES converges to an optimal parameter set X^* within the bounded search space, yielding identified hydrodynamic coefficients c_0 – c_4 for each

Algorithm 2 CMA-ES Based Fluid Coefficient Identification in MuJoCo

- 1: **Input:**
 - 2: Target trajectory T_{real} from real experiments
 - 3: Initial parameter guess \mathbf{x}_0
 - 4: Parameter bounds $[\mathbf{b}_{\min}, \mathbf{b}_{\max}]$
 - 5: Maximum evaluations N_{max}
 - 6: **Output:**
 - 7: Optimized fluid coefficients \mathbf{x}^*
 - 8: Load real trajectory data and construct target trajectory matrix T_{real}
 - 9: Initialize CMA-ES with dimension $D = 15$, step size σ_0 , and population size λ
 - 10: Initialize evaluation cache \mathcal{C}
 - 11: **while** not converged **and** $n < N_{\text{max}}$ **do**
 - 12: Generate candidate solutions $\{\mathbf{x}_k\}$
 - 13: **for** each candidate \mathbf{x}_k **do**
 - 14: Enforce physical and boundary constraints on \mathbf{x}_k
 - 15: Update MuJoCo XML fluid coefficients
 - 16: Run simulation and sample trajectory T_{sim}
 - 17: Compute MSE loss L_k
 - 18: Cache evaluation results
 - 19: **end for**
 - 20: Update CMA-ES distribution
 - 21: **end while**
 - 22: **return** best parameters \mathbf{x}^*
-

link. This parameter set minimizes the mean squared trajectory discrepancy over the entire time horizon.

By incorporating the identified coefficients into the MuJoCo model, we obtain the final calibrated underwater simulation model. The resulting model reproduces the experimentally observed motion patterns and dynamic responses without further manual tuning, serving as the baseline simulation model for subsequent analysis and real-to-sim validation.

III. REAL-TO-SIM UNDERACTUATED MECHANISM EXPERIMENTS

To evaluate the generalization capability of the identified hydrodynamic parameters and the fidelity of the calibrated simulation model, we conducted four independent experiments across two system configurations: the active–passive coupled mechanism and the purely passive mechanism. For each configuration, two distinct initial poses were tested. The results are presented in Figs. 4–7.

For each experimental group: Fig. (a) shows the initial pose of the real system; Fig. (b) shows the corresponding initial pose in simulation with the identified parameters; Fig. (c) illustrates the overall link motion in the real experiment, generated by superimposing frame-wise trajectory points extracted using SAM2; Figs. (d), (e), and (f) present the time-series trajectories of keypoints P_1 and P_2 , and P_3 , respectively. In the trajectory comparison plots, the blue solid lines denote real-world measurements, while the red dashed lines represent simulation results using the identified parameter set.

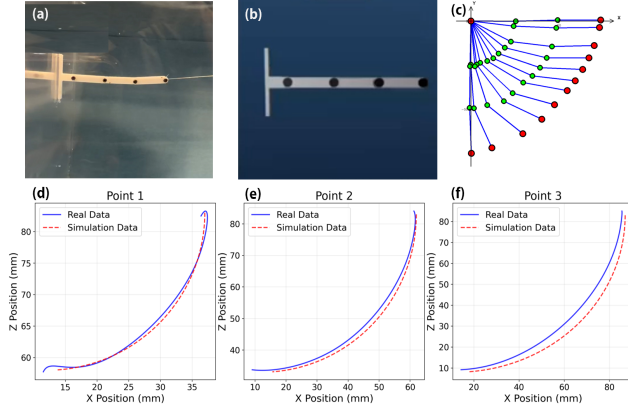


Fig. 4. Horizontal three-link trajectories: extracted vs. real data

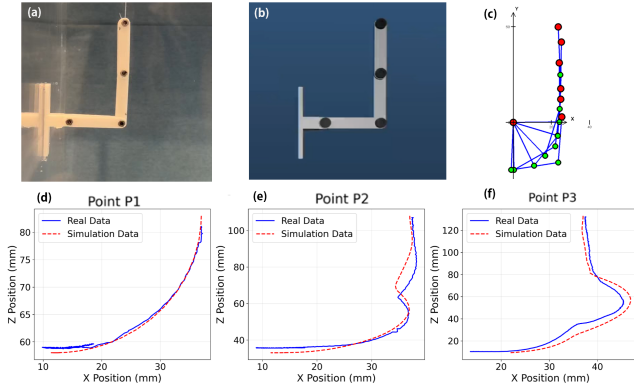


Fig. 5. Right-angle three-link trajectories: extracted vs. real data

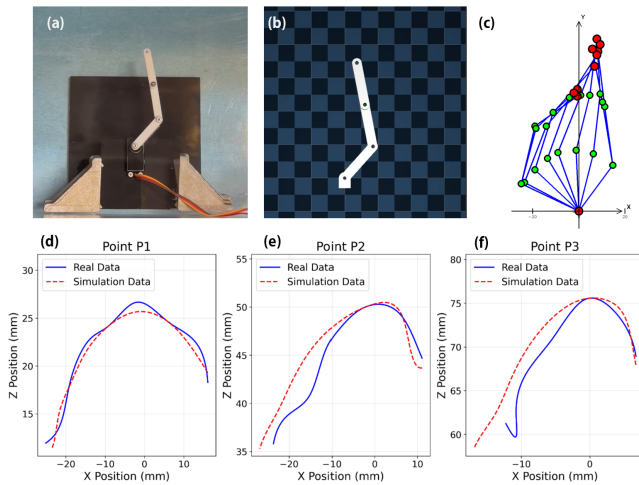


Fig. 6. Motor-driven three-link pose I: extracted trajectories vs. real data

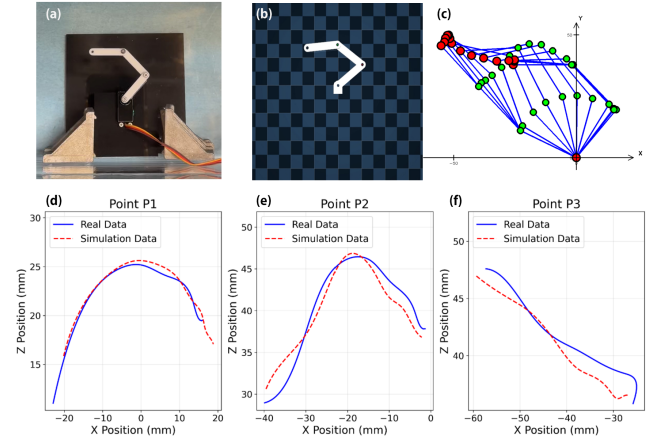


Fig. 7. Motor-driven three-link pose II: extracted trajectories vs. real data

In the real-to-simulation calibration process, the MuJoCo model incorporates both directly specified physical parameters and parameters identified through the proposed optimization framework.

Several parameters are assigned based on known physical properties or standard simulation settings. For the underwater environment, the fluid viscosity is directly specified according to the experimental conditions. For the actuation system, motor-related parameters including the velocity constant k_v and the force range are directly adopted from the actuator specifications. For the rigid-link structures, collision-related properties are enabled to allow geometric collision detection within the simulation environment.

The key parameters identified by the proposed method are the hydrodynamic coefficients governing the interaction between the links and the surrounding fluid. Specifically, five fluid coefficients (c_0-c_4) are optimized using the CMA-ES based identification framework described in Section II-C. These parameters characterize the dominant hydrodynamic forces acting on each link and are estimated by minimizing the trajectory discrepancy between the simulated and real-world motion data. In addition, joint damping and friction loss parameters are also identified to ensure stable numerical integration and realistic mechanical behavior.

By integrating the mechanical parameters with the identified hydrodynamic coefficients, the resulting MuJoCo model forms the final calibrated simulation system used for the subsequent real-to-sim validation experiments.

Across all four experimental scenarios, the calibrated simulation model consistently reproduces the motion trends and spatial evolution observed in the real system under varying initial conditions. In the active-passive configuration, the amplitude modulation of the distal keypoint P_2 and P_3 closely match experimental observations. In the purely passive configuration, the gravity-driven oscillatory decay behavior is likewise captured by the simulation model.

These results demonstrate that the proposed trajectory-based parameter identification method achieves not only trajectory fitting for a single experiment but also robust real-to-

sim consistency across varying initial conditions, indicating strong physical validity and generalization capability of the identified parameters.

Table I summarizes the average trajectory errors across the four experimental configurations. The error metric is defined as the Euclidean distance between simulated and real keypoint positions under time-aligned conditions, averaged over the entire trajectory duration.

TABLE I
UNDERACTUATED ROBOT COMPONENT RESULTS

Case	P1	P2	P3
Purely Passive Case 1	0.87	1.53	2.79
Purely Passive Case 2	1.35	1.76	2.54
Active-Passive Case 1	1.62	2.78	2.55
Active-Passive Case 2	1.14	1.97	1.68

In the experimental mechanism, each link has a length of 30 mm, with an overlap radius of 5 mm between adjacent links, resulting in an overall effective length of approximately 80 mm. Normalizing the trajectory error relative to this characteristic system length provides a physically meaningful performance indicator.

Across all four initial conditions, the overall average error remains below 5% of the total system length. Considering the strong nonlinear fluid–structure coupling and high-dimensional parameter space inherent to underwater underactuated mechanisms, this error level indicates that the identified hydrodynamic parameters accurately capture the real dynamic behavior.

These results validate the effectiveness and robustness of the proposed trajectory-based parameter identification method for underwater underactuated mechanisms and establish a reliable modeling foundation for extending the approach to fully actuated underwater robotic systems.

IV. SOFT ROBOT COMPONENT EXPERIMENT

In the previous sections, the proposed physical parameter identification method demonstrated strong performance on an underwater underactuated three-link mechanism. In this section, the method is further extended to an actual underwater soft robotic component to evaluate its applicability and generalization capability in complex flexible structures and interactive fluid dynamics.

Under the same active–passive actuation strategy, the original three-link mechanism is replaced by a single arm of an octopus-inspired robot (see Fig. 8(a)). The arm consists of eight serially connected segments with gradually decreasing width along its length, forming a tapered morphology. Compared with the rigid three-link mechanism, this structure exhibits higher degrees of freedom and stronger nonlinear fluid–structure coupling effects, significantly increasing the difficulty of physical parameter identification.

During underwater locomotion, the octopus-inspired arm demonstrates clear direction-dependent motion characteristics. When the direction of motion changes, both the velocity and posture differ, while the overall motion maintains a 2:1

velocity ratio. Specifically, the duration of the servo-driven counterclockwise motion is twice that of the clockwise motion. Fig. 9(a) and Fig. 9(b) illustrate the real experimental results. It can be observed that during counterclockwise motion, the arm undergoes significant bending deformation, whereas during clockwise motion, the arm remains relatively straight while swinging back.

Using the previously identified underwater fluid dynamic parameters, the simulation experiments were conducted under the same temporal conditions as the real system. Fig. 9(c) and Fig. 9(d), together with the supplementary experimental video, present the simulation results. The simulation not only successfully reproduces the 2:1 velocity ratio but also accurately captures the direction-dependent postural variations. Under identical time conditions, the simulated and real motions exhibit high consistency, with clear one-to-one correspondence throughout the motion process.

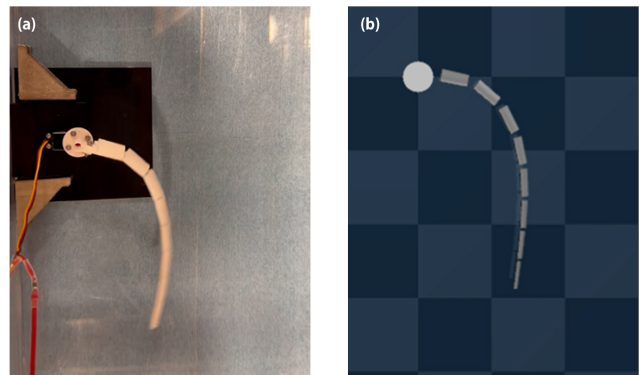


Fig. 8. Soft robot component prototype and its MuJoCo simulation model

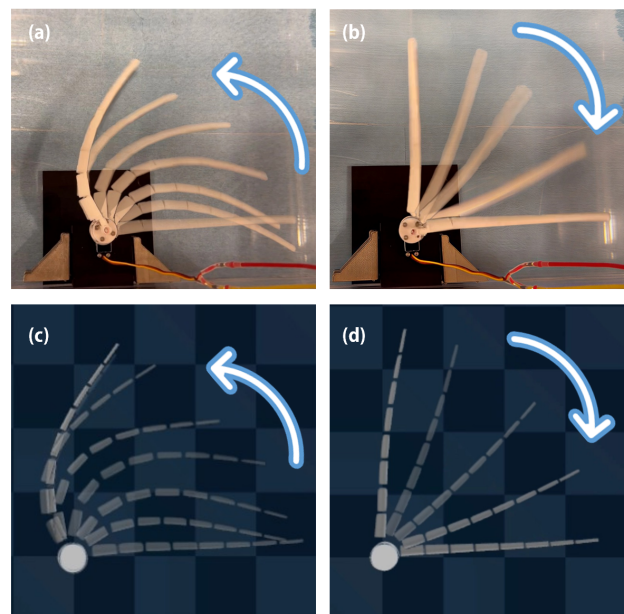


Fig. 9. Soft robot component motion: prototype vs. MuJoCo simulation

Fig. 10(a) and Fig. 10(b) adopt the previously described

Real-world Trajectory Extraction method, where the distal endpoint of the fourth segment is defined as P_1 , and the tip of the entire arm is defined as P_2 . These results (Fig. 10(c) and Fig. 10(d)) indicate that the proposed physical parameter identification method is not limited to underactuated rigid mechanisms but can also effectively model the dynamic behavior of complex flexible driven components in underwater environments, thereby providing a foundation for its application in underwater robotic systems.

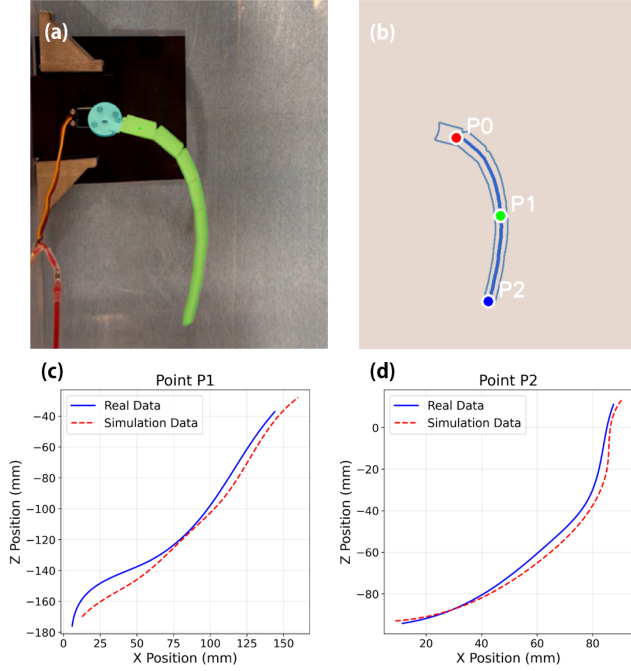


Fig. 10. Soft robot component: extracted trajectories vs. real data

V. SOFT ROBOT EXPERIMENT

After achieving satisfactory validation results on the single robotic arm, the proposed physical parameter identification method was further extended to the full robot body. Based on structural designs reported in the literature, a complete octopus-inspired underwater robot was constructed (see Fig. 11(a)), consisting of a central body platform and eight identical soft arms.

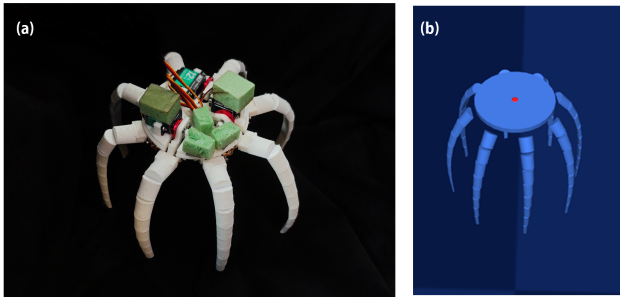


Fig. 11. Octopus-inspired soft robot prototype and its MuJoCo simulation model

In the full-body simulation model, the previously identified fluid dynamic parameters of a single arm were directly applied to all eight arms. A synchronized actuation strategy was adopted to drive the arms simultaneously. Through comparative experiments between the real robot and the simulation model (see Fig. 12), it can be observed that the simulated robot exhibits motion patterns, postural evolution, and propulsion characteristics highly consistent with those of the physical robot. This demonstrates that the identified parameters maintain good generalization capability and stability in a multi-actuator coupled system.

It should be noted that, under identical temporal conditions, the simulated robot achieves a slightly shorter displacement than the real robot. This discrepancy is primarily attributed to the fact that only the arm structures were subjected to physical parameter identification, while the central body platform (the octopus head) was not calibrated for fluid dynamic parameters. Since the platform also contributes additional mass and hydrodynamic drag effects during underwater locomotion, the unmodeled dynamics accumulate over time, resulting in reduced simulated displacement.

Despite this difference, the overall motion trends and postural evolution remain highly consistent, further validating the scalability and engineering applicability of the proposed physical parameter identification method to complete underwater robotic systems.

VI. CONCLUSIONS

In this work, we propose a unified physical parameter identification method for underwater underactuated systems, enabling consistent real-to-sim transfer from simplified mechanisms to complete robotic platforms. Unlike conventional sequential identification strategies, the proposed approach simultaneously estimates multiple fluid dynamic parameters within a single framework, thereby avoiding error accumulation and parameter coupling distortions introduced by stepwise calibration.

Overall, the results confirm that accurate physical parameter identification plays a critical role in bridging the real-to-sim gap for underwater robotic systems. The proposed method achieves system-level dynamic fidelity without relying on sequential parameter tuning or isolated calibration procedures, offering an efficient and broadly applicable solution for modeling and control of complex underwater underactuated robots.

Future work will focus on global hydrodynamic parameter identification of the complete robot structure, including the central body platform, and on integrating closed-loop control strategies to establish a high-precision, real-time underwater robotic simulation and control framework.

VII. ACKNOWLEDGMENT

The authors acknowledge the use of AI-assisted tools, including ChatGPT and Cursor, during the preparation of this manuscript. These tools were utilized to support tasks such as language refinement, figure preparation (Fig. 1, Fig. 4-7), and assistance in experimental code development. All

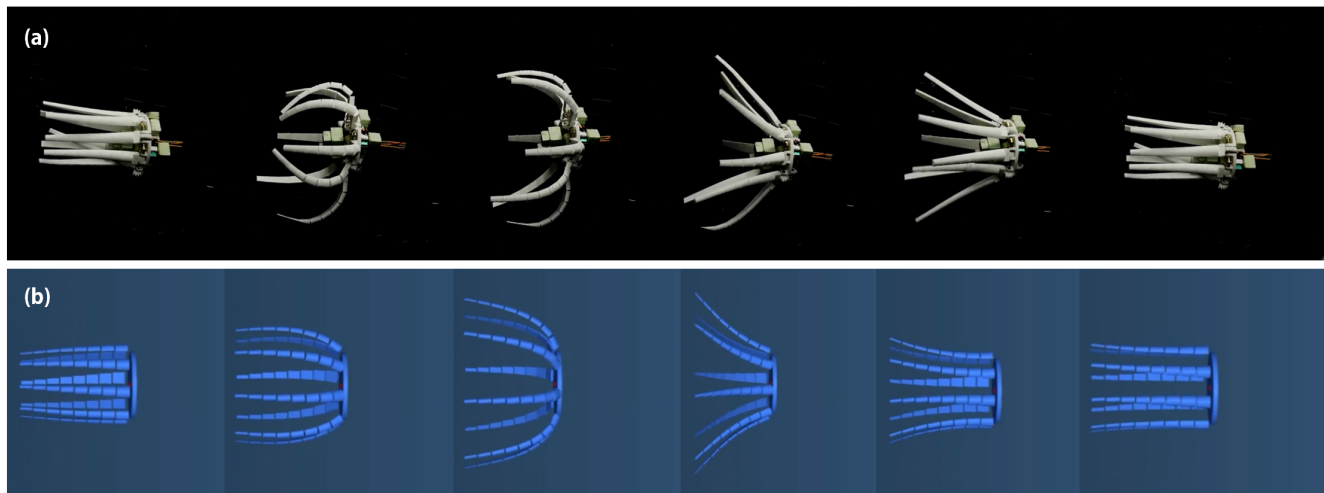


Fig. 12. Octopus-inspired soft robot motion: prototype vs. MuJoCo simulation

technical content, experimental design, results analysis, and conclusions were developed and verified by the authors.

REFERENCES

- [1] E. Ramirez-Llodra, A. Brandt, R. Danovaro, B. De Mol, E. Escobar, C. R. German, L. A. Levin, P. Martinez Arbizu, L. Menot, P. Buhl-Mortensen, B. E. Narayanaswamy, C. R. Smith, D. P. Tittensor, P. A. Tyler, A. Vanreusel, and M. Vecchione, "Deep, diverse and definitely different: Unique attributes of the world's largest ecosystem," *Biogeosciences*, vol. 7, no. 9, pp. 2851–2899, Sep. 2010.
- [2] O. Khatib, X. Yeh, G. Brantner, B. Soe, B. Kim, S. Ganguly, H. Stuart, S. Wang, M. Cutkosky, A. Edsinger, P. Mullins, M. Barham, C. R. Woolstra, K. N. Salama, M. L'Hour, and V. Creuze, "Ocean One: A Robotic Avatar for Oceanic Discovery," *IEEE Robotics & Automation Magazine*, vol. 23, no. 4, pp. 20–29, Dec. 2016.
- [3] A. Mazzeo, J. Aguzzi, M. Calisti, S. Canese, F. Vecchi, S. Stefanni, and M. Controzzi, "Marine Robotics for Deep-Sea Specimen Collection: A Systematic Review of Underwater Grippers," *Sensors*, vol. 22, no. 2, p. 648, Jan. 2022.
- [4] E. Morgan, I. Carlucho, W. Ard, and C. Barbalata, "Autonomous Underwater Manipulation: Current Trends in Dynamics, Control, Planning, Perception, and Future Directions," *Current Robotics Reports*, vol. 3, no. 4, pp. 187–198, Dec. 2022.
- [5] A. Mazzeo, J. Aguzzi, M. Calisti, S. Canese, F. Vecchi, S. Stefanni, and M. Controzzi, "Marine robotics for deep-sea specimen collection: A systematic review of underwater grippers," *Sensors*, vol. 22, no. 2, p. 648, 2022.
- [6] J. Wang, P. Du, Y. Zhang, Z. Xie, and C. Laschi, "From shallow waters to Mariana Trench: A survey of bio-inspired underwater soft robots," *Bioinspiration & Biomimetics*, 2026.
- [7] L. Li, B. Qin, W. Gao, Y. Li, Y. Zhang, B. Wang, S. Kong, J. Wang, D. He, and J. Yu, "Bioinspired underwater soft robots: From biology to robotics and back," Aug. 2025.
- [8] C. Armanini, M. Farman, M. Calisti, F. Giorgio-Serchi, C. Stefanini, and F. Renda, "Flagellate Underwater Robotics at Macroscale: Design, Modeling, and Characterization," *IEEE Transactions on Robotics*, vol. 38, no. 2, pp. 731–747, Apr. 2022.
- [9] A. T. Mathew, D. Feliu-Talegon, A. Y. Alkayas, F. Boyer, and F. Renda, "Reduced order modeling of hybrid soft-rigid robots using global, local, and state-dependent strain parameterization," *The International Journal of Robotics Research*, vol. 44, no. 1, pp. 129–154, Jan. 2025.
- [10] C. Laschi, "Modeling embodied intelligence: Can we capture its essence by modeling internal and external interactions?" *IOP Conference Series: Materials Science and Engineering*, vol. 1292, no. 1, p. 012001, Oct. 2023.
- [11] X. Liao, C. Zhou, Q. Zou, J. Wang, and B. Lu, "Dynamic Modeling and Performance Analysis for a Wire-Driven Elastic Robotic Fish," *IEEE Robotics and Automation Letters*, vol. 7, no. 4, pp. 11174–11181, Oct. 2022.
- [12] D. Chen, Z. Wu, H. Dong, M. Tan, and J. Yu, "Exploration of swimming performance for a biomimetic multi-joint robotic fish with a compliant passive joint," *Bioinspiration & Biomimetics*, vol. 16, no. 2, p. 026007, Dec. 2020.
- [13] Y. Zhong, Q. Wang, J. Yang, and C. Wang, "Design, Modeling, and Experiment of Underactuated Flexible Gliding Robotic Fish," *IEEE/ASME Transactions on Mechatronics*, vol. 29, no. 3, pp. 2266–2276, Jun. 2024.
- [14] J. Liu, Z. Zhu, and L. Wen, "Underwater soft arm grasping with simplified control using octopus-inspired bending propagation," *npj Robotics*, vol. 4, no. 1, p. 2, Jan. 2026.
- [15] C. Armanini, F. Boyer, A. T. Mathew, C. Duriez, and F. Renda, "Soft Robots Modeling: A Structured Overview," *IEEE Transactions on Robotics*, vol. 39, no. 3, pp. 1728–1748, Jun. 2023.
- [16] Z. Wang, N. M. Freris, and X. Wei, "SpiRobots: Logarithmic spiral-shaped robots for versatile grasping across scales," *Device*, vol. 3, no. 4, Apr. 2025.
- [17] H. Huang, J. Klusmann, H. Wang, S. Ji, F. Ying, Y. Zhang, J. Nassour, G. Cheng, D. Rus, J. Liu, M. H. Ang, and C. Laschi, "Physical Human-Robot Interaction for Grasping in Augmented Reality via Rigid-Soft Robot Synergy," Feb. 2026.
- [18] E. Todorov, T. Erez, and Y. Tassa, "MuJoCo: A physics engine for model-based control," in *2012 IEEE/RSJ International Conference on Intelligent Robots and Systems*, Oct. 2012, pp. 5026–5033.
- [19] Z. Wang, "Openspirobs: Open spiral robots toolkit," 2026. [Online]. Available: <https://github.com/ZhanchiWang/Open-Spiral-Robots>
- [20] N. Sobanbabu, G. He, T. He, Y. Yang, and G. Shi, "Sampling-based system identification with active exploration for legged sim2real learning," in *9th Annual Conference on Robot Learning*, 2025. [Online]. Available: <https://openreview.net/forum?id=UTPBM4dEUS>
- [21] B. Zhang, Y. Zhang, Y. Li, S. Xuan, H. W. Ng, Y. Liufu, Z. Tang, and C. Laschi, "Octopus-Swimming-Like Robot with Soft Asymmetric Arms," in *2025 IEEE 8th International Conference on Soft Robotics (RoboSoft)*, Apr. 2025, pp. 1–8.
- [22] N. Ravi, V. Gabeur, Y.-T. Hu, R. Hu, C. Ryali, T. Ma, H. Khedr, R. Rädle, C. Rolland, L. Gustafson *et al.*, "Sam 2: Segment anything in images and videos," 2024.